Magnetic resonance studies of chemically intercalated Li$_x$V$_2$O$_5$ aerogels

P. E. Stallworth, F. S. Johnson, S. G. Greenbaum, et al.

View Online   Export Citation

ARTICLES YOU MAY BE INTERESTED IN

Metal and ligand hyperfine couplings in transition metal complexes: The effect of spin–orbit coupling as studied by coupled perturbed Kohn–Sham theory
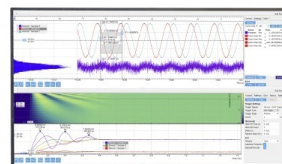The Journal of Chemical Physics **118**, 3939 (2003); https://doi.org/10.1063/1.1540619

Direct characterization of the Li intercalation mechanism into α-V$_2$O$_5$ nanowires using in-situ transmission electron microscopy
Applied Physics Letters **110**, 213903 (2017); https://doi.org/10.1063/1.4984111

Magnetic resonance studies of chemically intercalated $Li_xV_2O_5$ aerogels

P. E. Stallworth, F. S. Johnson, and S. G. Greenbaum[a)]
Department of Physics, Hunter College, City University of New York (CUNY), New York, New York 10021

S. Passerini
Ente per le Nuove Technologie, L'Energia e L'Ambiente (ENEA), Electrochemical Energy Conversion Division, C.R. Casaccia, Via Anguillarese 301, 00060 Rome, Italy

J. Flowers
Department of Physical, Environmental and Computer Sciences, Medgar Evers College of CUNY, Brooklyn, New York 11225

W. Smyrl
Corrosion Research Center, Department of Chemical Engineering and Material Science, University of Minnesota, Minneapolis, Minnesota 55455

^7Li, ^{51}V solid-state nuclear magnetic resonance (NMR) and electron paramagnetic resonance (EPR) measurements have been performed upon chemically lithiated $Li_xV_2O_5$ aerogels, with compositions of $1.00 < x < 5.84$. These compounds can intercalate reversibly large amounts of Li^+ and, therefore, are of interest as battery cathodes. Still, the mechanism regarding the electron transfer from an inserted lithium metal to a host aerogel V_2O_5 and details regarding the lithium cation environments are not fully understood. $Li_xV_2O_5$ crystals are known to exhibit various structural phase changes and, when multiple phases are present, the capability of the material to intercalate reversibly appears to be adversely affected. On the other hand, aerogels have no such multiphase behavior and aerogel based cathodes exhibit greater stability upon cycling. NMR shows that neither the structure nor the dynamics vary greatly with the amount of lithium content, and that the lithiated aerogel is best described as a single-phase material. Characterization of lithium and vanadium sites is performed through analysis of both NMR and EPR spectra. ^7Li line shapes are affected by first-order quadrupolar, magnetic dipolar interactions and motional narrowing. At and above room temperature, relaxation is governed primarily by a quadrupolar mechanism. NMR derived activation energies and diffusion coefficients are different from those of bronzes and electrochemically intercalated V_2O_5. ^{51}V NMR lines, indicative of the presence of V^{5+} at all compositions, undergo diamagnetic shifts of up to about 50 ppm with an increase in lithium content. These results imply the presence of oxidized impurities or electronic charge delocalization. Additionally, EPR measurements provide evidence of VO^{2+} impurities and indirect evidence of nonbridging oxygen at high lithium contents. © *2002 American Institute of Physics.* [DOI: 10.1063/1.1503171]

I. INTRODUCTION

There is much technological interest in $Li_xV_2O_5$ and other intercalation transition metal oxides because of their application as cathodes in rechargeable batteries.[1] Cathodes made from crystalline V_2O_5 can intercalate reversibly one Li^+ per V_2O_5 over many cycles; however, insertion of larger amounts of Li results in degradation of their performance. Recently, in order to increase the capacity, efforts have led to the processing of V_2O_5 aerogel (ARG) materials. These materials demonstrate remarkable properties that make them useful in a variety of electronic applications.[2] By supercritically drying the vanadium pentoxide hydrogel, ARG materials can be prepared in which the interconnected solid network typical of the gel state is preserved. The material is disordered and has a very high surface area and very thin solid phase thickness (10–20 nm). Further, ARG materials are microporous and the pore size reflects the liquid pore region of the original liquid gel. Thus the porous structure of the ARG can be easily manipulated through processing of the liquid gel. Technological focus is placed on the high surface areas (>400 m^2/g) and pore sizes (~ 2.3 cm^3/g), since these have a direct bearing upon the capacity. V_2O_5 ARG has the highest specific capacity of any vanadium oxide. Up to 5.8 equivalents of lithium per mole of V_2O_5 can be inserted by means of chemical lithiation. The high specific capacity (>650 mA h/g) also corresponds to a very high specific energy indicating that the ARG processing through supercritical drying fundamentally changes the nature of the insertion sites and yields a thermodynamically better host for Li insertion.

In previous work it was proposed that the enhancement of the electrochemical properties is due to the very large interlayer spacing together with a very thin solid phase.[3] This combination of properties allows the ARG to be a nearly two-dimensional host with very little interaction between adjacent layers. Still, the insertion mechanism in the ARG has

[a)]Author to whom correspondence should be addressed; electronic mail: steve.greenbaum@hunter.cuny.edu

not been fully characterized, especially regarding details of how the ARG accommodates electrons and lithium ions during cycling. The simplest picture associates the incorporation of lithium into the host with the reduction of vanadium from V^{5+} to V^{4+}. If insertion proceeds with at most two coexisting vanadium oxidation states for any given composition, then the reduction will proceed smoothly from V^{4+} to V^{3+}. However, this simple picture is compromised if electron delocalization, impurity phase formation or disproportionation of vanadium species occurs. For example, the creation of VO^{2+} ions is generally associated with the insertion of large amounts of lithium ($x > 2$) in crystalline V_2O_5. Also, electron paramagnetic resonance (EPR) and electron nuclear double resonance studies performed on crystalline $Li_xV_2O_5$, produced electrochemically, chemically, or by high-temperature methods,[4,5] showed that at lower lithium contents unpaired electrons become delocalized over two or four vanadium sites in the vicinity of lithium ions and that substantial covalent character exists between adjacent host layers. X-ray absorption spectroscopy and x-ray photoelectron spectroscopy measurements on ARG and xerogel materials show that the average vanadium oxidation state is not monotonically reduced upon lithium insertion and that partial electron delocalization occurs.[6,7]

There now exists a number of Raman spectroscopy, EPR, x-ray diffraction, nuclear magnetic resonance (NMR), and electrochemical studies performed on crystalline materials that illustrate the complex and sensitive link between the structure and the method of fabrication. These reports have all shown that the crystalline material maintains several structural phases that are dependent upon the lithium content, namely α, β, ε, γ, δ, ζ, etc.[4,5,8–18] The relative stability of these phases depends both on the lithium content and the fabrication conditions. Likewise, it is of interest to investigate the connection between properties, composition, and fabrication method. Specifically, the study presented here focuses on those $Li_xV_2O_5$ materials prepared via chemical intercalation means.[16,19,20]

At and above the micron scale, the V_2O_5 ARG is disordered; however, at smaller scales of $10^1 – 10^2$ nm the material forms ribbon-like structures. At even smaller scales the structure has been postulated to be a highly interconnected network of $[V_2O_5]_n$ bilayers comprised of axially distorted VO_5 edge-sharing pyramids.[21] Upon intercalation, Li ions are accommodated within the region between adjacent bilayers at apical oxygen sites. As shown in Fig. 1, each bilayer consists of two V_2O_5 sheets that face each other at a distance of about 0.28 nm.[21–23] This layered structure is similar to that found in δ-$Ag_xV_2O_5$.[24] The formation of the bilayer structure allows the vanadium atoms to also be coordinated with a sixth oxygen that belongs to the V_2O_5 sheet facing it. This sixth oxygen, however, also belongs to the base of the square planar VO_5 pyramid on the second sheet and is not an apical ($V{=}O$) oxygen as in crystalline V_2O_5. The interlayer distance in the pure V_2O_5 ARG (~ 1.25 nm) has been shown to be larger than in crystals of V_2O_5 and $V_2O_5 \cdot (0.5)H_2O$, and this difference could be due in part to retention of solvent in the ARG. The related xerogel material is formed through drying of the precursor gel, and it is during this process that
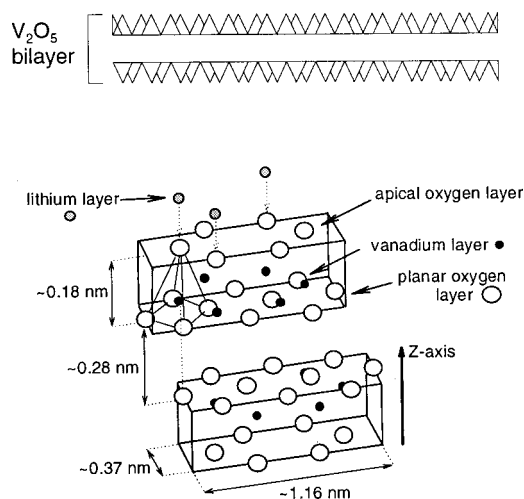

FIG. 1. Top: Bilayer structure of gel-based V_2O_5 materials. Triangles represent VO_5 pyramid units. Bottom: Illustration of the bilayer unit. The VO_5 pyramid unit is shown interacting with an oxygen from the nearby second layer. At low lithium content ions occupy symmetric sites in the layers near apical oxygen atoms. Not shown is the lithium layer associated with the lower V_2O_5 sheet.

large scale ribbon-like fibers (~ 10 nm wide and ~ 100 nm long) are created. Presumably some variant of these fiber structures exists in supercritically dried ARG materials.

It has been postulated that V_2O_5 ARG can accommodate more Li than its crystalline counterpart, due to larger interlayer distances and reduced interlayer interactions.[25] Structural modification of the V_2O_5 host through lithiation that adversely affects the material is thereby reduced. Additionally, the enhanced Li capacity could arise from large numbers of Li associated with VO_y surface defect states that exist in proportion to the surface area.[26] Within these disordered ARG materials a large number of defect states exist, yet in order for Li association to be useful, the defect chemistry must necessarily be reversible. A more satisfying explanation would include a description of the charge transfer mechanism from the inserted lithium to the host.

In order to work towards a more complete understanding of ARG materials, it is necessary for fundamental studies to be carried out first. Structural and dynamical information will naturally provide a foundation towards understanding the enhanced performance of ARG based cathodes. Presented here are the results of NMR and EPR measurements obtained for $Li_xV_2O_5$ ARG samples where $x = 1.00$, 2.01, 3.01, 3.79, 4.05, 4.91, and 5.84. The aim of this work is to characterize the Li and V sites in terms of their compositional and thermal dependencies. For the reasons given above the results we have gathered are expected to differ from those of crystalline compounds. Relevant spectroscopic parameters to be compared with corresponding values previously determined for bronzes, electrochemically and chemically intercalated $Li_xV_2O_5$ crystalline compounds, include quadrupolar coupling constants, chemical shifts, dipolar widths, spin-lattice relaxation rates, activation energies, diffusion coefficients, and g-tensor principal components.

II. EXPERIMENT

A. Sample preparation

Vanadium pentoxide gel was synthesized by ion exchange processing of sodium metavanadate (Fluka).[27] Aerogels were obtained by exchanging the water for acetone (EM Science, high purity) and then liquid CO_2 (Airgas, high purity).[25] Finally, conventional supercritical drying with liquid CO_2 (1200 psi at 32 °C) was carried out. The last two steps in the ARG processing were done using a Samdri 780A (Tousimis Research Corporation) supercritical drying apparatus. Chemical lithiation of the ARG material was carried out by reaction with *n*-butyl lithium.[19,20] The reaction enables one to determine the full capacity of an intercalation material in a simple and direct way; however, it has been pointed out that with this method some impurities can be created due to overreduction.[16]

The following procedure was used. *N*-butyl lithium (Aldrich, 1.6 M in hexane) was restandardized by titration with a standard HCl solution. A known quantity of the ARG sample was placed in a reaction vessel filled with an inert gas. A selected amount of *n*-butyl lithium was then introduced into the vessel by injection using an air-tight syringe. The mixture was allowed to react for 1 week to ensure complete lithiation. The liquid was extracted from the reaction vessel and hexane was injected several times to rinse out unreacted *n*-butyl lithium from the residue. The extracted solution was reacted with 2-propanol and the product (LiOH) was titrated with standard HCl using a phenolphthalein indicator. The difference between injected and unreacted *n*-butyl lithium corresponds to the amount of lithium intercalated into the sample. The filtered solid was analyzed for the Li/V molar ratio by atomic absorption/inductively coupled plasma (ICP) analysis. There was excellent agreement between the titration and elemental analysis results.

Chemical lithiation was very facile with the microporous V_2O_5 material. By reacting appropriate quantities of *n*-butyl lithium with the aerogel material, arbitrary compositions with specific stoichiometries of $Li_xV_2O_5$ of x ranging from 0 to 5.84 were prepared. The resultant ARG samples varied in color, depending on the lithium content: brownish red for the unlithiated sample, whereas the lithiated materials appeared dark green at $x=1$ and 2, and charcoal gray at larger lithium contents. NMR ready samples were prepared inside a drybox under argon gas. About 40 mg of the respective aerogel was packed into 5 mm Pyrex tubes with airtight Teflon plugs that secured the ends. A smaller amount of material was packed into 7 mm zirconia rotors for magic-angle spinning (MAS) measurements. Each sample was prepared for the EPR measurements by merely placing the entire filled 5 mm Pyrex tube and endcaps inside a 10 mm EPR tube. During the course of variable temperature measurements, samples were heated to 473 K in N_2 gas and a change in color indicative of reduction was observed: dark green for the unlithiated V_2O_5 ARG and charcoal gray for all the lithiated samples.

Concerning possible water content in the samples, no contamination at the source was present and the samples were prepared in a dry room in sealed bottles. To ensure zero water content, the samples were dried just prior to chemical lithiation. In this way, the *free* water content in the V_2O_5 aerogel is about zero. Any residual water (hydroxyl) can be extracted by low heating. For instance, extraction of H_2O, coming from hydroxyl groups at bilayer edges, is illustrated by the following reaction:

$$\{\cdots-(V_2O_5)_n-\cdots\}-OH+HO-\{\cdots-(V_2O_5)_m-\cdots\}\Rightarrow$$

$$\{\cdots-(V_2O_5)_n-\cdots-O-\cdots-(V_2O_5)_m-\cdots\}+H_2O.$$
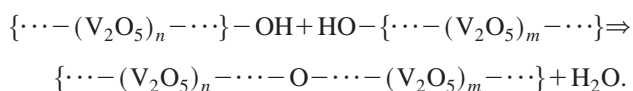
With conversion of terminal hydroxyl units to bridging oxygen atoms, adjacent bilayer fragments join and an overall reduction of surface area results.[25]

B. NMR and EPR measurements

Variable temperature ^7Li ($I=3/2$) NMR measurements were performed on a Chemagnetics CMX 300 spectrometer operating at 116.99 MHz (field strength of 7.1 T). The spectra were gathered using both phase cycled *pulse*-delay-acquire (one pulse) and *pulse-τ-pulse-τ*-acquire (two pulse, $25\ \mu s<\tau<50\ \mu s$) sequences followed by Fourier transformation of the free-induction decay or the trailing half echo. ^7Li MAS measurements were performed at 6 kHz to remove most of the broadening. At room temperature, excitation pulse lengths of 2.0 μs gave maximum signal strengths (e.g., a central transition $\pi/2$ pulse) and deadtime delays of 7.0 μs or more were employed. Variable temperature measurements 123–473 K range were carried out by channeling dry N_2 gas, at the desired temperature, through the NMR probe to the sample. Depending upon the temperature, sufficient time (2–10 s) was allowed following each scan to prevent saturation. Significant broadening of the line occurred at lower temperatures and the corresponding excitation pulse length was reduced to about 1.4 μs. ^7Li spin-lattice relaxation measurements were gathered using a 50 pulse saturation-train sequence: *pulse-τ$_{(sat)}$-...-pulse-τ$_{(sat)}$-pulse-t$_{(rec)}$*-acquire, where $\tau_{(sat)}=150\ \mu s$. The signal intensity, as a function of recovery time $t_{(rec)}$, was exponential only at higher temperatures. Aqueous LiCl (1.0 M) was used as the ^7Li reference and polycrystalline $LiVO_3$ (Alfa Aesar) was the solid standard.

^{51}V ($I=7/2$) NMR 295 K spectra, gathered at 79.18 MHz using a phase cycled two-pulse sequence ($50\ \mu s<\tau<100\ \mu s$), exhibited broad satellite responses (>250 kHz), and therefore pulse lengths of 1.0 μs were used in order to obtain reasonable excitation profiles and properly phased lines. For comparison, the $\pi/2$ pulse for the liquid standard $VOCl_3$ (Aldrich) was about 2.5 μs. V_2O_5 (Aldrich), VO_2 (Alfa Aesar), and V_2O_3 (Aldrich) were used as ^{51}V solid-state references.

EPR measurements were performed at 295 K on a Bruker EMX EPR spectrometer and the spectra were obtained in single field-sweep mode using a Bruker ER 4102ST X-band cavity. The resonance frequency for the cavity and sample in these experiments was between 9.60 to 9.63 GHz. Good signal to noise was obtained by employing a modulation amplitude of 1 G and modulation frequency of 100 kHz. Intensities were corrected for effects due to varying receiver

gain and/or microwave power on each sample. Spectral analyses were performed using WINEPR SIMFONIA Ver. 1.25 line shape simulation software.[28]

III. RESULTS AND DISCUSSION

A. ^{7}Li NMR

1. Spectra

For intensity comparisons, a known amount of LiVO$_3$ was chosen due to its comparable ^{7}Li linewidth and quadrupolar interaction. The NMR spectra from the ARG samples were integrated and normalized by the number of lithium nuclei in the sample according to the conditions described in Ref. 29. Assuming all ^{7}Li nuclei are represented in the LiVO$_3$ spectrum, the results show that for Li$_x$V$_2$O$_5$ compositions of $1 \leqslant x \leqslant 3.79$, 95% or more of all lithium nuclei are accounted for, yet at larger lithium contents the percentage of detected ^{7}Li nuclei reduces from about 95% at $x=4.05$ to roughly 80% at $x=5.84$. The lost signal is presumed to be the result of very strong interactions between ^{7}Li nuclei and paramagnetic centers. Comparisons made between spectra gathered from one-pulse and two-pulse sequences that employed a variety of excitation pulse widths (1–5 μs) and delays (50–200 μs) indicate that one-pulse data were affected by transient instrument response (after the pulse), and after corrections, resultant spectra gave somewhat narrowed features. Two-pulse data, on the other hand, gave exaggerated intensities for the first-order quadrupolar broadened satellite transitions.

ARG powder pattern lines, shown in Fig. 2, reveal symmetries typical of first-order quadrupole broadening but do not show resolvable second-order features or chemical shift anisotropy. The peak and center-of-gravity (COG) positions, both near 0 ppm, are weakly dependent upon the composition and virtually independent of the temperature within the range studied. Line shapes are affected by motional narrowing which is significant even at 295 K for lower lithium contents. In general, dipolar widths increase and the satellites become pronounced as x increases from 1 to 3.01. Little change occurs at higher lithium contents and the line shapes appear very similar to that at $x=3.01$. The ^{7}Li MAS spectra for all samples given in Fig. 3 show a single response near 0 ppm, typical of ionic lithium, with no evidence of metallic lithium (~ 260 ppm). Lithium environments are distributed, as explained below, but on average ARG sites are ionic and axially symmetric. Understanding the nature of distributions throughout the composition range of $0 < x < 5.84$ is important since the capability of a cathode to intercalate reversibly, as crystal studies have shown, is dependent upon the type and homogeneity of the phase.

In the case of symmetric and slightly asymmetric ^{7}Li environments, estimates of the magnitude of the quadrupolar coupling constant (usually defined in terms of the nuclear quadrupole moment, Q, the z component of the electric-field gradient eq and Planck's constant h: $Q_{cc}=e^2qQ/h$) can be obtained by taking twice the frequency width between the satellite divergences. However, with the ARG materials, the static responses have large distributions and the divergence positions are correspondingly obscured. Quadrupolar param-
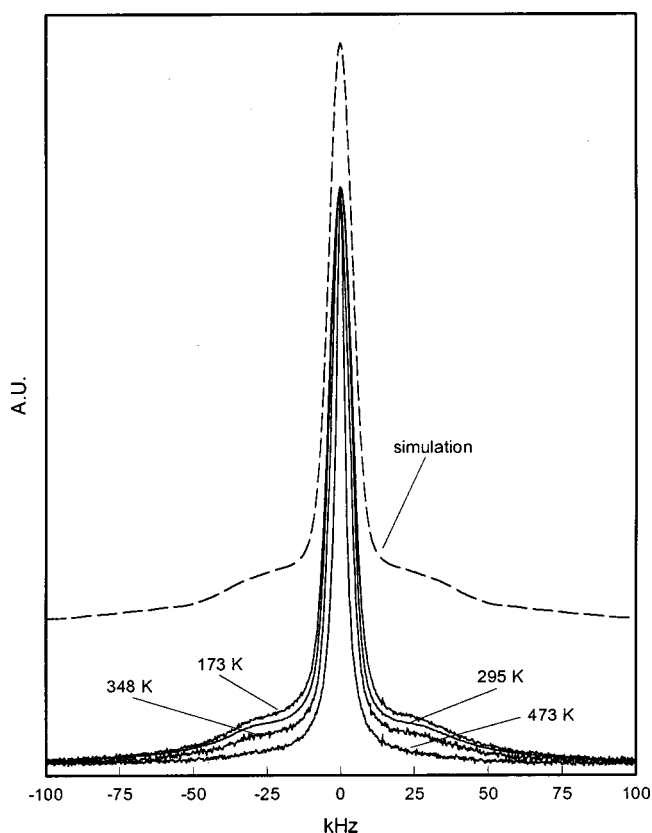

FIG. 2. ^{7}Li variable temperature one pulse spectra for Li$_{3.79}$V$_2$O$_5$ ARG. The top dotted line is the 173 K simulation.

eters which identify lithium environments can be extracted more effectively via line shape simulation. This procedure is carried out by calculating NMR powder pattern frequencies using a sum of interaction terms as perturbations of the larger Zeeman interaction.[30] Additional adjustments for the relative intensities of the central and satellite transitions of the simulated line shapes are made in order to facilitate a direct comparison with experimental pulse spectra.[31] $|Q_{cc}|$ and necessarily η, the quadrupolar asymmetry parameter, are distributed and efforts made to characterize the influence of each on the gathered line shapes demonstrated that quadrupolar features arise primarily from a more significant distribution in $|Q_{cc}|$. The tolerance in η is about 0.1 (which is taken as the half width of its distribution) and reasonable simulations were obtained by fixing η values per each $|Q_{cc}|$ distribution.

The low-temperature (123 K) line shape data have been simulated using two distinct distributions for $|Q_{cc}|$. These are represented by Gaussian (G) and Lorentzian (L) functions and are based on a simple two-component partition, illustrated in Fig. 4. The relative intensities of the component lines are sensitive to the composition. Essentially, $G(|Q_{cc}|)$ is characterized by $0 \leqslant \eta \leqslant 0.2$; its $|Q_{cc}|$ distribution is described by expression (1) with the peak value within the range 146 kHz$\leqslant \langle |Q_{cc}| \rangle \leqslant$156 kHz and standard deviation of $\sigma_{Q_{cc}}=24.5$ kHz.

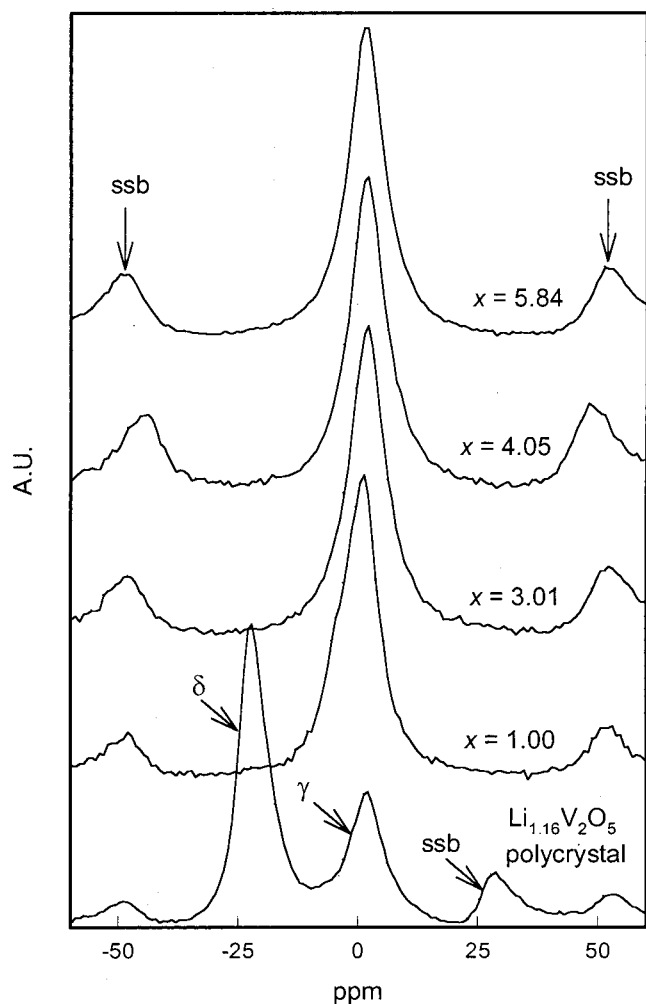$$G(|Q_{cc}|) \propto \exp\left(-\frac{(|Q_{cc}|-\langle |Q_{cc}| \rangle)^2}{2\sigma_{Q_{cc}}^2}\right). \quad (1)$$

FIG. 3. ^{7}Li MAS spectra of representative samples; ssb denotes spinning side band. Li$_{1.16}$V$_2$O$_5$ polycrystal data from Ref. 18.

FIG. 4. ^{7}Li ARG $|Q_{cc}|$ distribution illustrating component line weights I_L and I_G. The inset gives weights for L and G components vs x.

For $L(|Q_{cc}|)$, η is zero, and its $|Q_{cc}|$ distribution is described by expression (2) with peak $\langle |Q_{cc}| \rangle \approx 0$ and half width half maximum of $\Delta_{Q_{cc}} \approx 141.4$ kHz:

$$L(|Q_{cc}|) \propto \frac{\Delta_{Q_{cc}}^2}{(|Q_{cc}| - \langle |Q_{cc}| \rangle)^2 + \Delta_{Q_{cc}}^2}. \qquad (2)$$

The reasons for using expressions (1) and (2) are solely due to the good fit and simple analysis afforded, yet greater significance may exist in identification of two distinct lithium sites. If this is the case, then about 73% or more lithium ions belong to the $L(|Q_{cc}|)$ distribution and the remaining ions belong to the narrower $G(|Q_{cc}|)$ distribution. The mean value for $|Q_{cc}|$ over all sites is roughly equal to the average value of the Gaussian distribution. Additional results from this analysis are summarized in Table I.

NMR results for lithium sites previously identified in crystalline Li$_x$V$_2$O$_5$ are now compared with the ARG results.[13,18] Both δ and γ phases are known to coexist in the composition range of $1.0 < x < 1.5$, and several spectroscopic studies have demonstrated that each phase gives a distinct signature depending upon the fabrication procedure.[4,10,11,13,18] The lithium environments in the two phases are different. For instance, δ sites exhibit smaller qua-
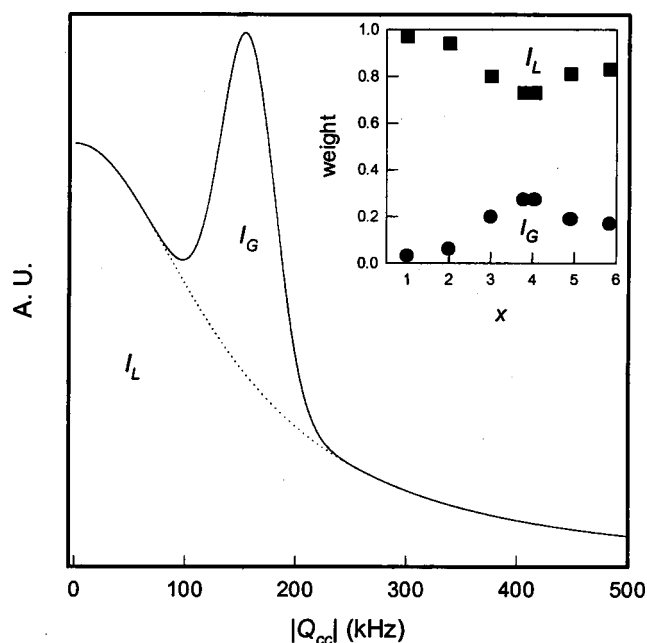
drupolar parameters ($|Q_{cc}| = 70–75$ kHz, $\eta \approx 0$), consistent with the proposed tetrahedral coordination to nearest neighbor oxygen atoms,[32] whereas γ sites, having octahedral coordination with significant distortions, exhibit larger quadrupolar parameters ($|Q_{cc}| = 120–130$ kHz, $\eta \approx 0.6$). Also, δ-LiV$_2$O$_5$ exhibits a more shielded ^{7}Li isotropic shift in the vicinity of -10 to -20 ppm, whereas the γ-LiV$_2$O$_5$ shift is about 0 ppm. Quadrupolar parameters for lithium sites in the ARG, particularly those of $G(|Q_{cc}|)$, are comparable to parameters associated with distorted octahedral sites in γ-LiV$_2$O$_5$, and as shown by the MAS data, the isotropic shift for the ARG materials is near 0 ppm. In this regard, ARG lithium sites identified by $G(|Q_{cc}|)$ appear to be more similar to those in γ-LiV$_2$O$_5$ than in δ-LiV$_2$O$_5$, even though $|Q_{cc}|$ values in the ARG are slightly larger. In contrast, the sites described by the $L(|Q_{cc}|)$ distribution are greatly varied and are not particularly characteristic of lithium sites in either δ- or γ-LiV$_2$O$_5$. Naturally, the $L(|Q_{cc}|)$ distribution can be identified with the structural disorder characteristic of the ARG lithium sites.

Further insight into the nature of lithium environments can be obtained via analysis of the magnetic dipole–dipole contributions. Typically, ^{7}Li NMR responses in reduced vanadates and other transition metal oxides are in general considerably broadened due to large dipolar coupling with nearby paramagnetic species (e.g., V^{4+}). The ARG responses are not as broad as those observed for either crystalline Li$_x$V$_2$O$_5$ or Li$_x$V$_6$O$_{13}$.[18,33] Estimates of the dipolar interaction strength, tabulated as standard deviation widths in Table I, were obtained by considering only homogeneous interactions using Gaussian convolutions of the bare quadrupolar broadened powder patterns. The dipolar widths quoted also include a contribution from the small spread of isotropic chemical shifts ($\sim$0.5 kHz half width measured from the MAS spectra). The discrepancies between measured and

TABLE I. ^{7}Li NMR simulation and BPP fitting results: $x=$ lithium content variable, $\sigma_D=$ simulated dipolar standard deviation, I_L and I_G are respective weights of Lorentzian and Gaussian partitions in $|Q_{cc}|$ distribution. $\Delta_{Q_{cc}}=$ Half width at half maximum of Lorentzian partition (141.4 kHz). $\langle|Q_{cc}|\rangle=$ Average electric quadrupole coupling constant for Gaussian partition. $\sigma_{Q_{cc}}=$ standard deviation of Gaussian partition (24.5 kHz). Δ_l and Δ_h are the respective limiting low- and high-temperature FWHMs used for the BPP fits. E_A values were obtained using $\tau_c=\tau_0\exp(E_A/k_BT)$ and Eq. (3). Uncertainties in the last digit of some values are indicated in parentheses.

Composition x	^{7}Li simulation results				BPP fitting results			
	σ_D (kHz)	I_L weight	I_G weight	$\langle|Q_{cc}|\rangle$ (kHz)	Δ_l (kHz)	Δ_h (kHz)	τ_0 (ns)	E_A (eV)
1.00	3.40(5)	0.97	0.03	156(2)	8.98	0.01	53.3	0.15
2.01	3.35(5)	0.94	0.06	156(2)	8.94	0.93	56.0	0.17
3.01	3.50(5)	0.80	0.20	146(2)	9.22	2.37	50.2	0.18
3.79	3.80(5)	0.73	0.27	146(2)	9.62	3.06	42.4	0.20
4.05	3.70(5)	0.73	0.27	146(2)	9.42	2.81	54.9	0.19
4.91	3.70(5)	0.81	0.19	156(2)	9.43	2.58	52.8	0.19
5.84	3.63(5)	0.83	0.17	156(2)	9.38	2.49	47.8	0.19

simulated widths are due to overlapping quadrupolar contributions ($0\leqslant|Q_{cc}|\leqslant20$ kHz) in the narrow center region of the static lines. ^{7}Li dipolar widths increase with lithium content up to $x=3.79$, after which they decrease slightly by about 5% from the maximum value (Fig. 6 inset). One explanation for the decrease after $x=3.79$ is that the layered structure of the V_2O_5 ARG host, which expands along the Z direction (Fig. 1) in order to accommodate more Li$^+$ ions, expands in the planar dimension as well. The expansion must be large enough to override increased numbers of ^{7}Li–^{7}Li, ^{7}Li–^{51}V, and ^{7}Li–V$^{3+,4+}$ magnetic interactions.

Additionally, a small paramagnetic shift of about 2 ppm is observed in the MAS spectra as the lithium content increases from $x=1$ to 3.01. As shown in Fig. 5, the shift does not change significantly throughout $3.01<x<5.84$. (Similar compositional trends are observed in the ^{51}V NMR and EPR results given below.) The shift, regardless of lithium content, has little temperature dependence, and overall these data show that paramagnetic effects on the ^{7}Li spectra are relatively weak.

2. Temperature dependence and relaxation

^{7}Li ARG responses are subject to motional narrowing, even though the shifts are not strongly temperature dependent, and the dipolar distribution gradually evolves from Gaussian to Lorentzian with an increase in temperature. For the moment, it is assumed with these disordered materials that there are no special restrictions on Li$^+$ motion (e.g., reduced dimensionality) and that the linewidth dynamics are for the most part effectively governed by a single thermally activated mechanism (lithium ions hop between sites located near apical oxygen positions). A Bloembergen–Purcell–Pound (BPP) analysis is employed as an approximation in order to describe the most basic trends.[34] The simplest approach allows extraction of the activation energy, E_A, using the correlation time given by $\tau_c=\tau_0\exp(E_A/k_BT)$ where k_B is the Boltzmann constant and T the temperature, along with the following formula:

$$\tau_c=\frac{C}{\Delta_e}\left(\tan\left[\frac{\pi}{2}\left(\frac{\Delta_e^2-\Delta_h^2}{\Delta_l^2-\Delta_h^2}\right)\right]\right). \quad (3)$$

Here Δ_e, Δ_h, and Δ_l are the experimental, limiting high-temperature, and limiting low-temperature fullwidth at half maximum (FWHM) values of the central transition, respectively, and the constant C is roughly equal to 0.2 for Gaussian and Lorentzian line shapes.

The temperature and compositional dependence of the FWHM is shown in Fig. 6 and the BPP results are given in Table I. Discrepancies are observed at temperatures greater than 350 K for samples $x=1$ and 2, and this is attributed to larger dipolar interactions due to chemical and structural transformations that the aerogel undergoes upon heating. As will be addressed in Sec. IIIB and C, there is evidence that
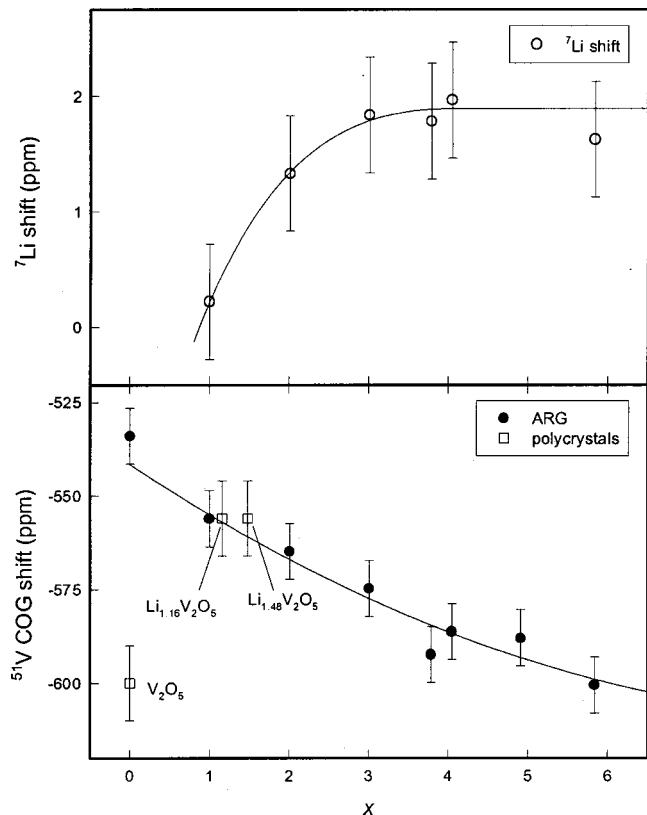

FIG. 5. Line shift vs x. Solid curves are guides to the eye. Top: ^{7}Li MAS isotropic shift vs x. Bottom: ^{51}V center-of-gravity vs x.
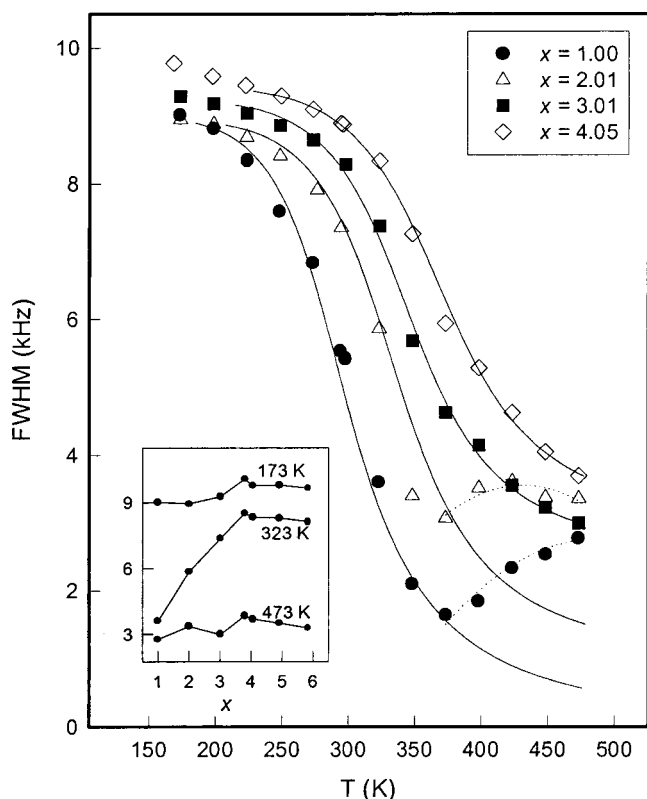
FIG. 6. ^{7}Li FWHM (full width at half maximum in kHz) data vs the temperature with BPP fits. Dotted lines denote the departure from BPP behavior for $x=1.00$ and 2.01. The inset shows the compositional dependence for some temperatures (FWHM vs x).

heating promotes the formation of V^{3+}. BPP formalism holds better for samples where $x>2$; since larger amounts of vanadium exist as V^{3+} anyway, heating has a lesser effect.

The results show little or no compositional dependence for τ_0, and its consistency (average value of about 51 $\times 10^{-9}$ s) probably reflects the similar nature of lithium sites (i.e., ionic) and the single-phase behavior of the V_2O_5 ARG host over the entire compositional range. Extracted E_A values, however, reveal a small compositional dependence. As shown in Table I, E_A initially increases from 0.15 eV with the lithium content, and then levels off at about 0.20 eV for $x \geq 3.79$. Since E_A depends upon the availability of sites to which excited lithium ions can jump, the number of such sites decreases with x and motion of any one ion becomes increasingly dependent upon the motion of others. It is interesting to note that E_A decreases with the lithium content for electrochemically lithiated $Li_xV_2O_5$ (containing 5 mol % P_2O_5) for $0.2 \leq x \leq 2$.[12] E_A values from ARG samples $x=1.00$ and 2.01 presented here are about 40% and 30% smaller than the respective samples in Ref. 12. Additionally, E_A for ARG sample $x=1$ is about 90% larger than that reported in Refs. 8 and 10 for $Li_{0.35}V_{1.98}O_5$ and γ-LiV_2O_5 bronzes, respectively. This variation illustrates again that the properties of $Li_xV_2O_5$ depend not just upon the composition but also upon the fabrication procedure.

Estimates of room temperature self-diffusion coefficients (D) are obtained using

$$D = \frac{l^2}{2d\tau_c}. \tag{4}$$

If isotropic motion is assumed then $d=3$ and the jump distance can be taken as the average length between the nearest apical oxygen sites ($l \approx 0.4$ nm). As the lithium content decreases from 5.84 to 1.00, $D_{295\,K}$ increases from about 2 $\times 10^{-12}$ to 13×10^{-12} cm^2/s. Also, since τ_0 is rather insensitive to x, the behavior of $D_{295\,K}$ merely reflects its dependence on E_A, and restates that of inhibited motion at larger lithium content. This result is very approximate particularly at large x due to the saturation of apical sites and resulting uncertainty of l. Again, the trend is opposite that observed for the electrochemically lithiated $Li_xV_2O_5$ containing 5 mol % P_2O_5.[12]

Spin-lattice relaxation rates were obtained from the recovery of the entire (integrated) Fourier transformed response following a saturation-pulse train. In this analysis all transitions are considered, unlike in the above linewidth analysis; consequently, the recovery profiles (as a function of recovery time) were generally observed to be nonexponential. In light of the dominant interactions found with ARG materials, quadrupolar contributions to relaxation can account for the nonexponential recovery (exponential behavior is expected for the recovery of an entire line in the event of dipolar relaxation). Such phenomena involve coupling between the ^{7}Li nuclear quadrupole moment and the surrounding electric field gradient (EFG), and the spin-lattice relaxation is fulfilled from the inherent link between the EFG and bonding electrons. The rates, W_1 and W_2, were extracted from saturation recovery data using the following expression (also see the Appendix):

$$\frac{N(t)}{N_\infty} = 1 - \left(\frac{f}{3}\right)e^{-2W_1 t} - \left(\frac{1+f}{3}\right)e^{-2W_2 t}, \tag{5}$$

where N_∞ is the equilibrium magnetization ($t=\infty$). The coefficient f exists within the range of 0 and 1 and depends upon the saturation conditions of the line. For all but a few recovery profiles it was found that f was greater than 0.95. The above expression takes into account any partial irradiation of the satellites, which is important if the line shape changes with the temperature. As was the case here, excitation pulse widths (corresponding to maximum signal intensity) generally increased and recovery profiles gradually tended towards single exponential behavior ($W_1 \approx W_2$) with an increase in temperature.

Arrhenius plots of $\ln(2W_{1,2})$ versus inverse temperature are shown in Fig. 7. Unlike the linewidth data, uncertainties in the relaxation rates preclude the identification of any compositional dependence. On the high-temperature side, the rates increase with the temperature; however, due to the high-temperature instability of the ARG a true characteristic maximum cannot be attained. This is in contrast to the behavior of $Li_{0.35}V_{1.98}O_5$ bronze, where a maximum in the rate is observed.[8] With the ARG samples at lower temperatures the rates are much less dependent on the temperature, and a paramagnetic dipolar relaxation mechanism becomes increasingly important. Consequently, the quadrupolar description specified by Eq. (5) is not entirely appropriate, and in
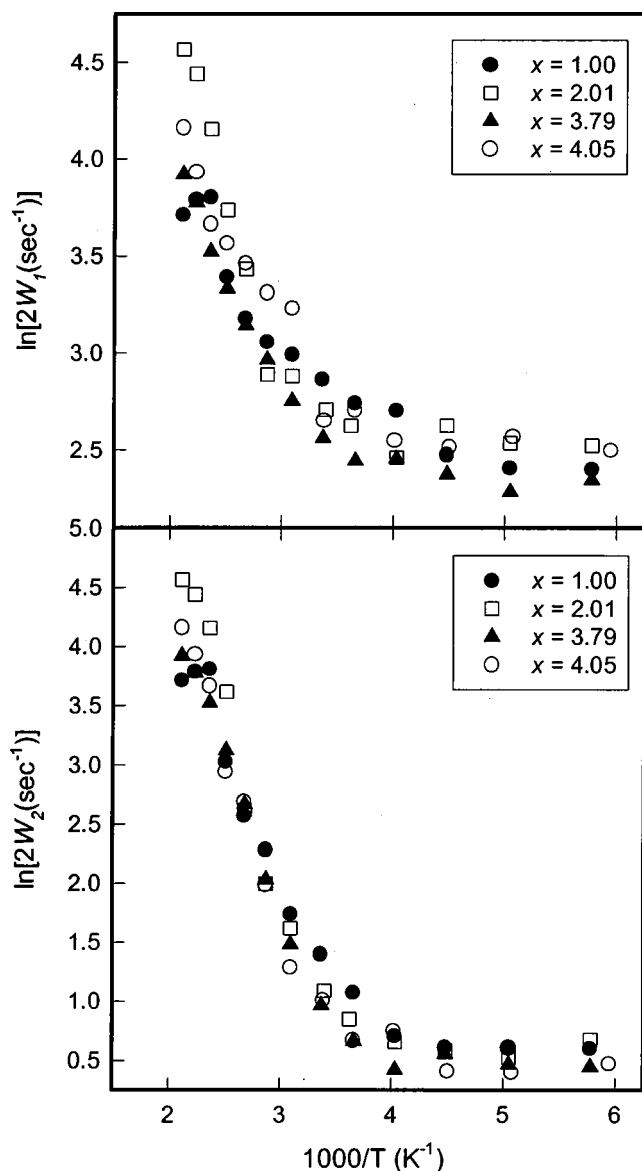
FIG. 7. Quadrupolar relaxation: ^{7}Li $\ln(2W_{1,2})$ vs $1/T$.

general the relaxation is described by at least two processes, depending on the respective temperature. Considering the stronger quadrupolar contribution at higher temperatures, the derivative of the $\ln(2W_1)$ profile obtained between $2.1 < 1000/T < 3.4$ yields an activation energy that is on the order of that found via linewidth behavior. This lends some credence to the BPP analysis even though restricted dimensionality effects have not been addressed.

B. ^{51}V NMR

Due to large magnetic dipolar interactions between the vanadium nuclear moment and localized electron moments, the ^{51}V NMR responses for V^{4+} and V^{3+} species ($3d^1$ and $3d^2$) are difficult or impossible to detect in solids using conventional pulsed NMR. This is true for the vanadium response of the vanadyl ion VO^{2+}. However, if there are no unpaired electrons or if the unpaired electron spins are largely decoupled from the vanadium nucleus then the ^{51}V resonance is normally observable. Such is the case with

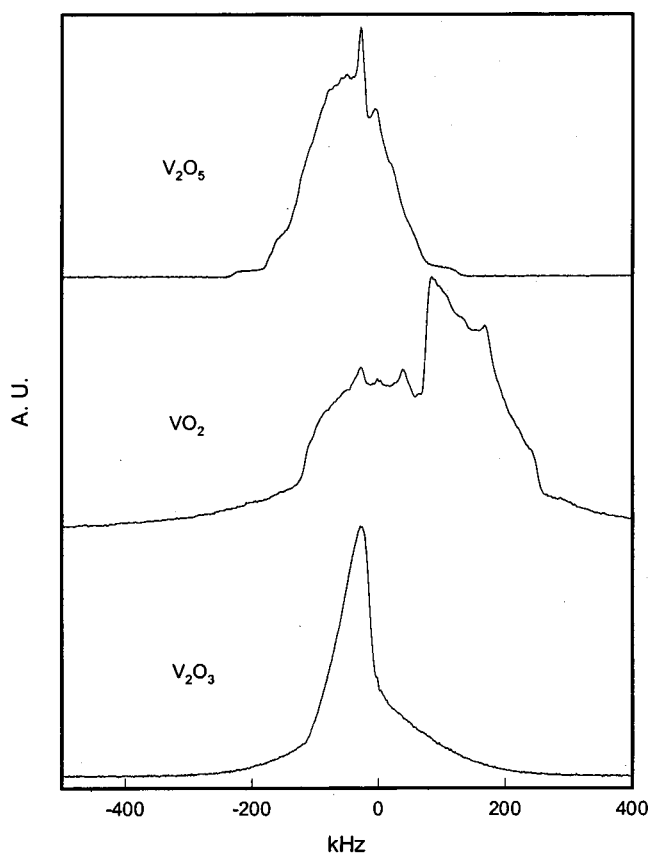FIG. 8. ^{51}V 295 K two pulse (echo) spectra of various oxide samples.

V_2O_5, VO_2, and V_2O_3, even though the nucleus–electron coupling scheme is different in each case. ^{51}V NMR studies have been performed on these compounds and their spectra are shown in Fig. 8. The study of these oxides may shed some light on the ^{51}V spectra of ARG materials.

With V_2O_5 each vanadium exists as $3d^0$, and therefore, the defect-free ^{51}V response is not affected by either paramagnetic or large nucleus–electron contact interactions. The ^{51}V spectrum of a polycrystalline sample is characterized by the following representative parameters: $|Q_{cc}| \approx 800$ kHz, $\eta \approx 0.2$, $\sigma_{xx} \approx \sigma_{yy} \approx -250$ to -320 ppm and $\sigma_{zz} \approx -1200$ to -1250 ppm.[35–37] Coupling of much larger magnitude has been reported for the ^{51}V line in VO_2.[38] In this oxide, when $T < 340$ K, structural distortions maintain closely spaced neighboring vanadium atoms and allow electron moments, donated from adjacent $3d^1$ vanadium species, to pair and participate in bonding configurations.[39,40] Apparently due to electron pairing, the room temperature ^{51}V signal is observable. The COG is greatly shifted by about $+1030$ ppm relative to ^{51}VOCl$_3$ and it is therefore speculated that the signal is influenced by large contact interactions. The behavior is in contrast to that of the negative (diamagnetic) shifts from V_2O_5 (~ -610 ppm) and V_2O_3 (~ -380 ppm). In the phase just above 150 K, V_2O_3 exhibits metallic properties since neighboring $3d^2$ vanadium species each contribute two electrons that are delocalized within two bands.[41] The NMR spectrum thereby exhibits Knight shifts which become less diamagnetic with an increase in temperature.[42] From the breadth of the satellites for V_2O_3 it is seen that its ^{51}V quad-
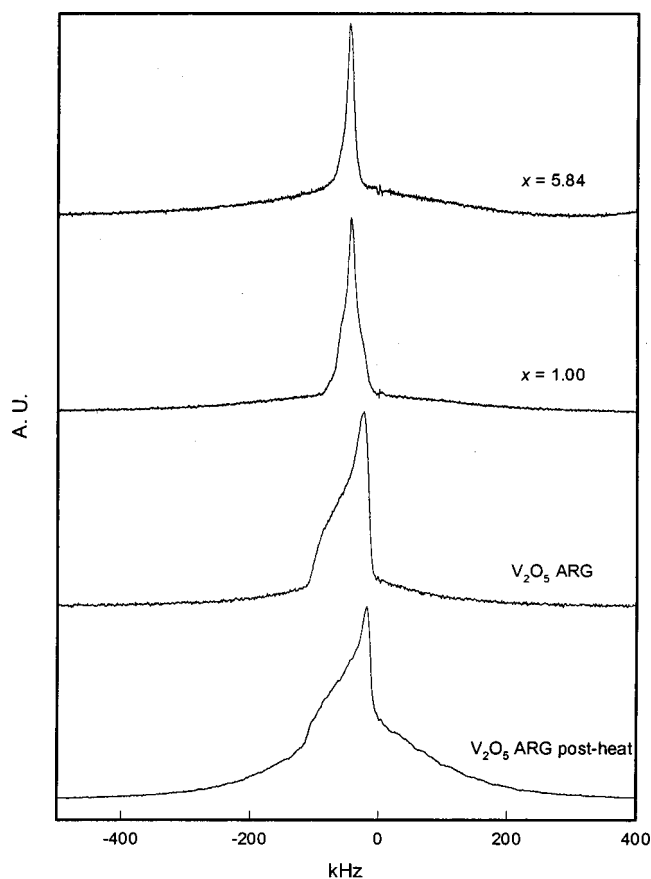
FIG. 9. ^{51}V 295 K two pulse (echo) spectra of lithiated and unlithiated ARG samples.

rupole interaction is comparable to that of V_2O_5.

Interactions represented in the ^{51}V spectra for the ARG materials could in part arise from pairing and/or delocalization of electron moments, as with VO_2 and V_2O_3, and additionally, may be due to V^{5+}-rich crystalline phases (e.g., δ- and γ-LiV_2O_5). The spectrum of the unlithiated V_2O_5 ARG shown in Fig. 9 is typical of chemical shift anisotropy with no discernable second-order quadrupolar effects. Simulation of the spectrum yields chemical shift tensor components that are fairly close to those of polycrystalline V_2O_5: $\sigma_{xx} \approx \sigma_{yy} \approx -220$ ppm and $\sigma_{zz} \approx -1280$ ppm, therefore, differences between the ARG and crystalline V_2O_5 structures are primarily reflected by quadrupolar details. The quadrupolar interaction is particularly sensitive to local perturbations of the EFG, whereas the chemical shift also includes contributions from beyond the first coordination sphere, and these are generally present in both crystalline and ARG materials. As discussed in Sec. I, an axially distorted VO_6 octahedron in the bilayer structure is an equally suitable description of vanadium environments in the ARG, and the spectral differences between the ARG and crystalline V_2O_5 are those pertaining to interlayer distances and the nature of the "sixth" oxygen on the adjacent sheet (e.g., apical or equatorial).

The spectrum changes dramatically upon incorporation of lithium into the V_2O_5 host. As shown in Fig. 9, the slightly asymmetric room-temperature ^{51}V responses display similarly broadened satellite components; however there is a

much narrower central transition about 20 kHz in width. There is little or no chemical shift anisotropy, the line shape is insensitive to the lithium content and considering the breadth of the satellites, the quadrupolar interaction appears to be at most of the order of that of the unlithiated ARG. These ^{51}V spectra are similar to those previously reported for chemically intercalated $Li_xV_2O_5$ polycrystals ($x=1.16$ and 1.48).[18] In that study, the spectral features from δ and γ phases were not distinct, yet differences in the satellite features of the two crystals were attributed to increased disorder in the host structure at larger lithium content. These sorts of differences in the ARG materials are not apparent since, beyond the nanometer-scale ribbon structure, the aerogels are fundamentally disordered at all compositions.

The ^{51}V intensity represents that fraction of vanadium nuclei whose resonant frequencies are not shifted and broadened beyond detection due to large couplings with localized unpaired electron moments. An estimate of the fraction of detectable nuclei may be obtained through normalization of the ^{51}V spectra. In analogy to the procedure used above to estimate the Li content, spectral intensities from ARG samples were compared with that of a known amount of V_2O_5. The results indicate that most vanadium nuclei remain undetected due to wipe-out effects from unpaired electron spins localized near ^{51}V nuclei. This leads to the conclusion that through lithium insertion the majority of vanadium atoms are reduced from V^{5+} to V^{4+} and V^{3+}, thereby the V^{5+} content for lithiated materials is dilute. Evidence concerning V^{3+} content will be discussed below. Roughly 25% of the potential vanadium signal is observed at $x=1$, following which the percentage drops to about 10% at $x=3.79$, and remains at this value throughout $3.79 \leq x \leq 5.84$. Considering the formal vanadium oxidation value $(10-x)/2$, the V^{5+} content is lower than expected at $x=1$, and higher than expected at $x>1$. The anomalously high V^{5+} content at large lithium contents could be attributed to oxidized defects or, as previously mentioned, crystalline phases that formed during sample preparation. These are not expected to be present in large quantity since procedures were taken to minimize exposure to atmospheric O_2. Moreover, impurity states are formed at the expense of the V_2O_5 host; their presence would adversely affect the material to intercalate reversibly.[4] It is unlikely, therefore, that large amounts ($>25\%$) of oxidized impurity phases are present since the ARG material demonstrates exceptional reversibility throughout most of the compositional range. If neighboring vanadium atoms were sufficiently close so as to allow some orbital overlap, then delocalization of electrons throughout manifolds composed of $3d$ atomic orbitals becomes possible. In this case, the ^{51}V signal may not reflect in a pure sense the V^{5+} oxidation state, as observed with VO_2 and V_2O_3, and the explicit assignments of V^{5+}, V^{4+}, and V^{3+} species are correspondingly obscured.

Figure 5 shows a small negative shift of about 50 ppm for the ^{51}V COG with an increase in x. Besides signal intensity, the shift is the most substantive difference between ^{51}V spectra for lithiated samples and is noteworthy since positive (yet temperature insensitive) shifts are observed in the ^{7}Li data. The ^{51}V linewidth of the central transition does not

change with the lithium content, as expected, following increased paramagnetic concentrations. Therefore a bulk susceptibility associated with localized moments cannot completely account for all trends. The fact that the ^{51}V shift is negative and apparently continuous implies that electron density and/or distortions evolve smoothly about the vanadium sites as the lithium content changes. These latter effects are not large enough to cause measurable differences in quadrupolar features however. The shift could arise from the action of traditional chemical shift mechanisms (i.e., diamagnetic electron currents) antiferromagnetic ordering of neighboring paramagnets (which could result in no shift or even a diamagnetic shift), or through core polarization effects due to d electrons. In order for core polarization to take place, a partial transfer of electronic charge would have to occur, e.g., delocalization between $3d^1$ and $3d^0$ neighboring vanadium species.[43]

The variable temperature measurements provided an opportunity to investigate the effect of heating on the ^{51}V NMR and EPR (see below). On average, the lithiated samples exhibited a 10% mass loss, which presumably indicates that some structural reorganization occurred with probable emission of O_2. Dramatic spectral effects were observed for the unlithiated V_2O_5 ARG, shown in Fig. 9, where heating caused an increase in the satellite distribution and a decrease in the shift. The resulting spectrum is similar to that of polycrystalline V_2O_3. For this and other evidence from EPR measurements given below, it appears that heating under anaerobic conditions promotes the transformation: V_2O_5ARG$\rightarrow V_2O_3 + O_2$. For lithiated samples, spectral intensities gathered before and after heat treatment were not substantially different for $x \leq 2$, but were different for larger lithium contents. The shape of the ^{51}V lines for lithiated samples were not affected by heating.

The shift of the ^{51}V COG, remeasured after heating, was about 21% smaller (less negative) for the V_2O_5 ARG and no more than 8% smaller for the lithiated samples. In a general sense, heating under N_2 appears to cause electrons to become localized at vanadium atoms and thereby the V^{3+} paramagnetic content becomes enhanced, regardless of lithium content. Additional considerations of thermal treatment include the impact on the surface area. For example, a reduced surface area could follow O_2 emission during heat treatment, in analogy with the emission of H_2O from hydrated V_2O_5 ARG. Such a treatment is likely to alter the content of defects and oxidized impurity phases and correspondingly the ^{51}V spectral intensities.

C. EPR

Determination of the fate of electrons donated to the V_2O_5 host upon lithium insertion is an important step towards characterizing the charge transfer mechanism. ^{51}V NMR gives a partial picture, indicating from the low spectral intensities that most electronic charge is localized, i.e., attributed to V^{4+} and V^{3+}. EPR can supplement NMR by providing a direct measure of V^{4+} and defect-related paramagnetic states. Direct observation of the V^{3+} species, however, is not favorable since very large zero-field contributions and other
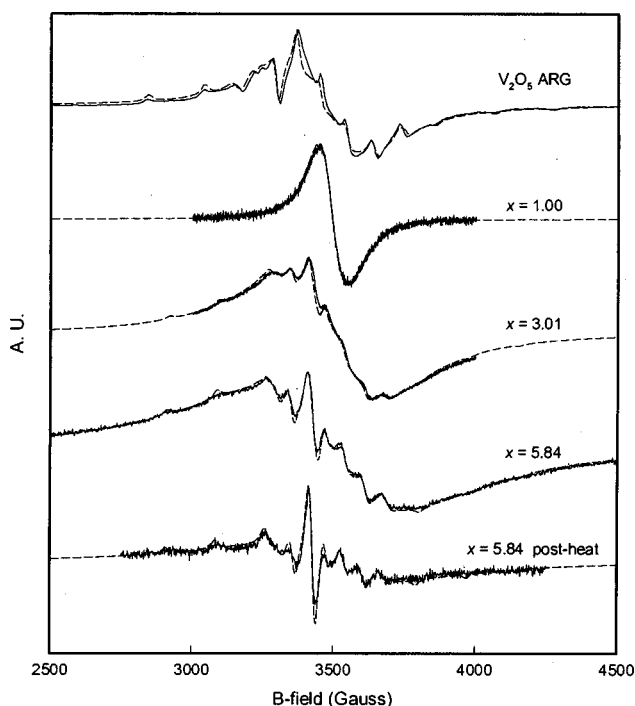

FIG. 10. EPR 295 K spectra of lithiated and unlithiated ARG samples. The simulations are shown as dashed lines.

strong relaxation mechanisms are expected for this $3d^2$ state. No substantial differences can be observed in the EPR spectra for samples $x \geq 3.79$, and therefore the paramagnetic V^{2+} ion (i.e., in VO) is considered to be absent in the ARG.

Two contributions are generally observed for ARG materials: a featureless broad component and a hyperfine component. In considering the lithiated samples, the broad line reflects a large distribution of V^{4+} states and accounts for more than 90% of the spectral intensity. The broad line also exhibits g_{iso} values close to those reported for δ- and γ-phase crystalline LiV_2O_5. The smaller hyperfine contribution is due to a dilute concentration of VO^{2+} species. The latter signature, which reveals eight transitions due to hyperfine coupling between the localized electron moment and a nearby ^{51}V nucleus ($I = 7/2$), has been unambiguously identified in diverse systems including electrochemically intercalated V_2O_5, vanadium containing oxide glasses, TiO_2-based catalysts, and zeolites.[4,44–46] EPR spectra obtained at 295 K are shown in Fig. 10. Details regarding the paramagnetic environments can be obtained through deconvolution and simulation of the powder pattern components. It is sufficient to consider only the Zeeman, second-order hyperfine and dipolar interactions; the latter can be incorporated through convolution of the bare powder patterns with Lorentzian broadening functions. Simulations were performed by inputting per site one set of nondistributed g values, weightings, hyperfine components ($A_\parallel$ and $A_\perp$) and peak-to-antipeak dipolar broadening widths (here $\Delta B_\parallel = \Delta B_\perp = \Delta B$). Continuous distributions in g values were unaccounted for, consequently these are considered the major differences between best fits and experimental spectra. The results, being generally good, are summarized in Table II.

TABLE II. EPR simulation results: Δ_B is defined as the peak–antipeak width of the derivative Lorentzian convolution function. Uncertainties in the last digits of some values are indicated in parentheses. Residual weights correspond to the VO^{2+} EPR signal intensity.

Composition x	ESR simulation results				ESR simulation results (postheating)			
	Δ_B (G)	Weight	$g_\perp$, $g_\parallel$	$A_\perp$, $A_\parallel$	Δ_B (G)	Weight	$g_\perp$, $g_\parallel$	$A_\perp$, $A_\parallel$ (G)
0.00	250(5)	0.930(2)	1.972, 1.972	0, 20	No signal	⋯	⋯	⋯
1.00	83(5)	~1.00	1.969, 1.948	0, 20	580(5)	~1.00	1.960, 1.960	0, 0
2.01	123(5)	~1.00	1.969, 1.948	0, 20	500(5)	0.950(5)	1.960, 1.960	0, 0
3.01	320(5)	0.982(2)	1.965, 1.948	0, 20	No measurement	⋯	⋯	⋯
3.79	575(10)	0.987(2)	1.965, 1.948	0, 20	No measurement	⋯	⋯	⋯
4.05	575(10)	0.986(2)	1.965, 1.948	0, 20	500(10)	0.920(5)	1.960, 1.960	0, 0
4.91	500(10)	0.987(2)	1.965, 1.948	0, 20	500(10)	0.930(5)	1.960, 1.960	0, 0
5.84	520(10)	0.985(2)	1.965, 1.948	0, 20	500(10)	0.950(5)	1.960, 1.960	0, 0

The dominant EPR line of the pure unlithiated V_2O_5 ARG spectrum is Lorentzian in shape with $\Delta B = 250$ G and $g_{iso} = 1.972$. Hyperfine parameters, beyond those of the VO^{2+} component, are considered to be distributed, very small, or absent. This signature arises from V^{4+} species in oxygen-deficient V_2O_{5-y} states and appears to be related to the Gaussian-broadened defect lines observed in polycrystalline V_2O_5 and $Li_{1.48}V_2O_5$.[18,45] The narrower features, associated with VO^{2+}, have been simulated with an axially symmetric g tensor. Here better fits of the data were obtained by introducing off-diagonal terms in the second-order hyperfine simulation. No quadrupolar interactions were considered. For the unlithiated material, the VO^{2+} site is characterized by $\Delta B \approx 17$ G $g_\perp \approx 1.980$, $g_\parallel \approx 1.922$, $A_{xx} \approx 80$ G, $A_{yy} \approx 90$ G, $A_{zz} \approx 200$ G, $A_{xz} \approx 10$ G, $A_{yz} \approx 20$ G, and $A_{xy} \approx 0$. Initially the VO^{2+} content is zero or very small; however, throughout the composition interval of $3 \leqslant x \leqslant 5.84$, this signal gradually increases with x to about 1.5% of the total intensity. The VO^{2+} sites are somewhat different for lithiated ARG materials: $\Delta B \approx 18-20$ G $g_\perp \approx 1.972-1.975$, $g_\parallel \approx 1.938-1.940$, $A_{xx} \approx 55-60$ G, $A_{yy} \approx 63-66$ G, $A_{zz} \approx 173-179$ G, $A_{xz} \approx 9-13$ G, $A_{yz} \approx 11-17$ G, and $A_{xy} \approx 0$ (and these values are susceptible to small variations with heat treatment). It is speculated that residual organics left over from fabrication, along with H_2O in the case of the unlithiated material, serve to complex the VO^{2+} ions, and therefore the nature of the VO^{2+} ion in the aerogel is that of an impurity. The broad EPR spectral line is identified as a characteristic aerogel signature.

The ARG signals for $Li_xV_2O_5$ are significantly different from those of the pure V_2O_5 ARG and therefore are distinct from those associated with V^{4+} in the V_2O_{5-y} paramagnetic defect states mentioned above. Instead, the spectra are attributed to V^{4+} ions residing within VO_5 pyramids of the characteristic ARG bilayer structure. At low lithium contents ($x = 1.00$ and 2.01), the cation association is through the apical oxygen of the pyramid unit and the single transferred electron is localized at the vanadium atom, forming a V^{4+} paramagnetic center. The paramagnetic centers are affected by distortions along the V–O–Li axis and the symmetry is reflected in both the g and hyperfine tensor components. The perpendicular component, $g_\perp$, decreases somewhat and the parallel component, $g_\parallel$, remains unchanged as the lithium

content increases from $x = 2.01$ to 3.01. The addition of more lithium beyond $x = 2.01$ results in a slight decrease of the axial distortion at the V^{4+} sites. For $x > 3.01$, the constancy of the g tensor indicates that the structure about the V^{4+} site does not vary.

ΔB generally depends on the paramagnetic concentrations and as expected increases with the lithium content. In the composition interval of $2.01 \leqslant x \leqslant 4.05$, the average V oxidation state is further reduced with an increase in lithium content, and the dramatic increase of ΔB can be attributed to larger paramagnetic interactions for the enhanced V^{3+} content. For compositions $x > 4$, ΔB decreases from its maximum value of ~ 570 to ~ 500 G (Table II). This is consistent with the proposed expansion as more lithium ions are accommodated into the structure. The formation of the V^{3+} oxidation state from V^{4+} and V^{5+} is expected to result in large distortions of the crystal field from octahedral as inferred by the oxide structures. Again like impurity phases, these perturbations on the aerogel structure should adversely affect the cyclability of the material. For these reasons, the V^{3+} content is probably smaller than expected (for example, less than 50% at $x = 3$). In light of disproportionation amongst vanadium oxidation states, it is speculated that for large x charge is compensated not only through V^{3+} formation but also through the formation of nonbridging oxygens on VO_5 structures, i.e., V–O–V links become attacked by inserted lithium ions thereby creating nonbridging ionic $Li^{+-}O-V$ terminations. In this way, the aerogel pyramid VO_5 units might be preserved within allowable distortions even at large x. This argument can be extended to address the unlikelihood of further reduction of the vanadium oxidation state below $3+$.

There are large differences in EPR spectra taken before and after heat treatment. The postheating EPR signal vanishes altogether for the unlithiated V_2O_5 ARG, where, as shown in Fig. 10 for the lithiated materials, the intensity for the broad line decreases about 5% relative to the VO^{2+} hyperfine component and ΔB levels off near 500 G for most compositions. In that the VO^{2+} content is enhanced slightly, the loss of intensity for the broad line reflects the diminished V^{4+} content and is consistent with the interpretation that upon heating some V^{4+} is converted to undetectable V^{3+}. Additionally shown in Table II is the effect of heating on the

g tensor for the surviving V^{4+} sites. The apparent symmetrizing (i.e., $g_\parallel = g_\perp = g_{iso}$) reflects a more relaxed structure and greater uniformity of the V–O bonds.

IV. CONCLUSIONS

Chemically lithiated $Li_xV_2O_5$ aerogels where $1.00 \leq x \leq 5.84$ have been studied via combined spectroscopies using ^7Li, ^{51}V NMR and EPR. The results show that the lithium environments in aerogels are generally different from both electrochemically lithiated and high-temperature bronze materials. First-order quadrupolar broadened ^7Li line shapes have been interpreted in terms of two distributions. A small minority of lithium sites are similar to those in γ-LiV_2O_5, whereas the majority of environments are widely distributed with $|Q_{cc}|$ varying by as much as 150 kHz or more. The wide distribution reflects the structural disorder characteristic of the ARG. All lithium sites are ionic, however, and have axial symmetry. This is consistent with structural interpretations previously given, at least for $x \leq 2.01$, that intercalated lithium ions are situated at apical oxygen positions between adjacent V_2O_5 bilayer sheets. Evidence of this type of ordering was provided by extended x-ray absorption fine structure (EXAFS) studies of chemically inserted Zn ions in a V_2O_5 ARG.[47] With the incorporation of larger amounts of lithium, saturation of apical oxygen positions occurs and residual lithium ions are forced to occupy alternative sites. Here it is speculated that lithium ions become associated with nonbridging oxygens in the equatorial plane of the VO_5 units. This conclusion is based on the absence of metallic lithium (^7Li NMR), the temperature dependent disproportionation of vanadium species (^{51}V NMR and EPR), and the lower than theoretical V^{3+} content (V^{4+} EPR signal, particularly for $x \geq 4.05$). No clear distinction in the spectra has been made between lithium ions associated with apical and nonbridging oxygens.

A BPP analysis of ^7Li lines yielded activation energies which increase from 0.15 to 0.20 eV with an increase in x and thereby suggests that ionic motion becomes more hindered for higher lithium contents. Differences between these activation energies (and diffusion coefficients) with those of bronzes and electrochemically intercalated V_2O_5 were noted. The temperature dependent ion dynamics appear to be similar at all compositions above $x = 2.01$, whereas for lower lithium content heating causes anomalous linewidth behavior that is most likely related to structural modifications. High-temperature treatment results in sample mass loss and enhancement of the V^{3+} content. Even though the paramagnetic content (V^{4+} and V^{3+}) is significant at all compositions, the coupling between ^7Li nuclei and paramagnets is relatively weak and is further reduced by motional averaging at room temperature.

The fact that ^{51}V NMR can be observed at all compositions is intriguing. In order to account for this effective V^{5+} signal, charge compensation requires some combination of the following: (1) delocalized electrons within bands comprised of $3d$ orbitals from neighboring vanadium atoms, (2) the presence of significant oxidized impurity phases ($\sim 10\%$), and (3) localized electron charges on oxygen atoms

(nonbridging). The most superficial differences between the unlithiated and lithiated materials indicate that the ^{51}V signal is dilute and that chemical shift effects are largely reduced in the latter. This interpretation along with that of structural expansion upon insertion particularly at large x (FWHM data) does not support the scenario of significant electron delocalization. The presence of a diamagnetic impurity phase similar to γ-LiV_2O_5 (as suggested by the G distribution of ^7Li $|Q_{cc}|$ values) may account for some if not all of the observed ^{51}V NMR.

It is well known that EPR allows identification of the VO^{2+} impurity, which is known to be particularly deleterious towards cycling over normal voltages. A small amount of this impurity is detected in ARG materials. The characteristic EPR signal from the ARG is broader and much more intense than that of the impurity VO^{2+}, and these lines are easily separated. The ^{51}V spectra from unlithiated and lithiated ARG materials are different, where unspecified V_2O_{5-y} defect states describe the former, whereas V^{4+} paramagnetic centers within VO_5 pyramid units define the latter. V^{3+} sites cannot be characterized here, and regarding this, magnetic susceptibility measurements would be of great value. The evolution of the ARG signature (g values) with x follows a host of other trends (^7Li shift, E_A, ^{51}V line shapes), in that the EPR spectra are virtually identical for $x \geq 3.79$. Again, an interpretation based on nonbridging oxygens is employed to account for the behavior at large x.

ARG materials are of such great interest, primarily because of their capacity, as well as chemical and structural stability with cycling. No significant multiphase behavior is observed, yet as seen through electrochemical measurements, electronic changes occur as lithium is inserted. Moreover, these electronic adjustments within the host are largely reversible. This has interesting consequences pertaining to the nature of charge transfer mechanisms between (1) lithium and vanadium via apical oxygens and (2) those purported between lithium and nonbridging oxygens. The results presented here indicate that the $Li_xV_2O_5$ ARG for the most part can be considered as a single nonstoichiometric "phase" and that lithium intercalates smoothly (at least for $x \leq 5.84$) into the V_2O_5 host as an ion.

APPENDIX

For quadrupolar relaxation in the case of nuclear spin $I = 3/2$, the transition probabilities between adjacent levels (W_1 for $\pm 3/2 \leftrightarrow \pm 1/2$) and the next outerlying levels (W_2 for $\pm 3/2 \leftrightarrow \mp 1/2$) must be considered. When the system is at equilibrium with the external field, the difference in population between adjacent nuclear levels is considered a function of temperature T and resonant energy $h\nu$. For the experi-

mental conditions presented in this article, the difference can be approximated as $N_m - N_{m+1} \approx (N_0 h\upsilon)/(4k_B T) = N_0 \Delta/4$ where the total population is $N_0 = \Sigma N_m$. The rate equation given by Ref. 48 is therefore

$$\frac{d\mathbf{N}(t)}{dt} = \mathbf{M} \cdot \mathbf{N}(t) + \frac{N_0 \Delta}{2} \mathbf{W}, \tag{A1}$$

where

$$\mathbf{N}(t) = \begin{pmatrix} N_{-1/2} - N_{-3/2} \\ N_{1/2} - N_{-1/2} \\ N_{3/2} - N_{1/2} \end{pmatrix}, \quad \mathbf{W} = \begin{pmatrix} W_1 \\ 2W_2 - W_1 \\ W_1 \end{pmatrix},$$

and

$$\mathbf{M} = \begin{pmatrix} -\dfrac{W_1}{2}(1+3\Delta) - W_2(1+2\Delta) & -W_1\Delta & -\dfrac{W_1}{2}\Delta + W_2 \\[2mm] \dfrac{W_1}{2}(2+\Delta) - W_2(1+\Delta) & -2W_2(1+\Delta) & \dfrac{W_1}{2}(2+\Delta) - W_2(1+\Delta) \\[2mm] \dfrac{W_1}{2}\Delta + W_2(1+2\Delta) & W_1\Delta & -\dfrac{W_1}{2}(4+\Delta) - W_2 \end{pmatrix}.$$

The eigenvalues of the nonsingular matrix $\mathbf{M}$ are $-2W_1$, $-2W_2$, and $-2(W_1+W_2)$ and Eq. (A1) can be recast in terms of the diagonalizing matrix $\mathbf{D}$,

$$\frac{d\mathbf{A}(t)}{dt} = \mathbf{D}^{-1}\mathbf{M}\mathbf{D} \cdot \mathbf{A}(t)$$

$$= \begin{pmatrix} -2W_1 & 0 & 0 \\ 0 & -2W_2 & 0 \\ 0 & 0 & -2(W_1+W_2) \end{pmatrix} \mathbf{A}(t). \tag{A2}$$

The exponential solutions for $\mathbf{A}(t)$ are used to obtain the population difference $\mathbf{N}(t)$ using,

$$\mathbf{N}(t) = \mathbf{D} \cdot \mathbf{A}(t) - \frac{N_0 \Delta}{2} \mathbf{M}^{-1} \cdot \mathbf{W}. \tag{A3}$$

The recovery behavior (**N**) depends upon the initial conditions of the spin system. For the experiments presented here, it is assumed that initially only the central transition is fully saturated and, due to possible inhomogeneous illumination of the line, the degree of saturation for the satellites is partial. To account for this, the parameter f is introduced into the solutions for $\mathbf{N}(t)$. When $f=1$ there will be complete saturation of the entire line, and when $f=0$ only the central transition will be saturated. Therefore, the state of the spin system immediately after application of the saturating pulse is written as

$$\mathbf{N}(0) = \begin{pmatrix} \dfrac{N_0 \Delta}{4}(1-f) \\[2mm] 0 \\[2mm] \dfrac{N_0 \Delta}{4}(1-f) \end{pmatrix}. \tag{A4}$$

Upon consideration of the symmetry of the first-order quadrupolar interaction, the initial satellite contributions are arbitrarily set equal to each other (since only their sum is sig-

nificant in this analysis). The recovery of the entire line given by Eq. (5) is the result of the normalized sum of the components of $\mathbf{N}(t)$.

[1] C. Julien and G.-A. Nazri, *Solid State Batteries: Materials Design and Optimization* (Kluwer Academic, Boston, 1994).
[2] D. R. Rolison and B. Dunn, J. Mater. Chem. **11**, 963 (2001).
[3] S. Passerini, W. H. Smyrl, M. Berrettoni, R. Tossici, R. Rosolen, R. Marassi, and F. Decker, Solid State Ionics **90**, 5 (1996).
[4] B. Pecquenard, D. Gourier, and N. Baffier, Solid State Ionics **78**, 287 (1995).
[5] B. Pecquenard, D. Gourier, and D. Caurant, J. Phys. Chem. **100**, 9152 (1996).
[6] S. Passerini, D. B. Le, W. H. Smyrl, M. Berrettoni, R. Tossici, R. Marassi, and M. Giorgetti, Solid State Ionics **104**, 195 (1997).
[7] M. Giorgetti, S. Passerini, W. H. Smyrl, S. Mukerjee, X. Q. Yang, and J. McBreen, J. Electrochem. Soc. **146**, 2387 (1999).
[8] J. Gendell, R. M. Cotts, and M. J. Sienko, J. Chem. Phys. **37**, 220 (1962).
[9] M. Bose and A. Basu, Solid State Ionics **18&19**, 902 (1986).
[10] J. M. Cocciantelli, K. S. Suh, J. Sénégas, J. P. Doumerc, J. L. Soubeyroux, M. Pouchard, and P. Hagenmuller, J. Phys. Chem. Solids **53**, 51 (1992).
[11] J. M. Cocciantelli, K. S. Suh, J. Sénégas, J. P. Doumerc, and M. Pouchard, J. Phys. Chem. Solids **53**, 57 (1992).
[12] T. Asai, S. Sugimoto, S. Kawai, S. Okada, and J.-I. Yamaki, MRS Bull. **24**, 75 (1989).
[13] J. Hirschinger, T. Mongrelet, C. Marichal, P. Granger, J.-M. Savariault, E. Déramond, and J. Galy, J. Phys. Chem. **97**, 10301 (1993).
[14] X. Zhang and R. Frech, J. Electrochem. Soc. **145**, 847 (1998).
[15] E. A. Meulenkamp, W. van Klinken, and A. R. Schlatmann, Solid State Ionics **126**, 235 (1999).
[16] D. W. Murphy, P. A. Christian, F. J. DiSalvo, and J. V. Waszczak, Inorg. Chem. **18**, 2800 (1979).
[17] J. M. Cocciantelli, J. P. Doumerc, M. Pouchard, M. Broussely, and J. Labat, J. Power Sources **34**, 103 (1991).
[18] P. E. Stallworth, F. S. Johnson, S. G. Greenbaum, S. Passerini, J. Flowers, W. Smyrl, and J. J. Fontanella, Solid State Ionics **146**, 43 (2002).
[19] D. W. Murphy, F. J. DiSalvo, G. W. Hull, Jr., and J. V. Waszczak, Inorg. Chem. **15**, 17 (1976).
[20] M. S. Whittingham, M. B. Dines, J. Electrochem. Soc. **124**, 1387 (1977).
[21] M. Giorgetti, S. Passerini, W. H. Smyrl, and M. Berrettoni, Inorg. Chem. **39**, 1514 (2000).
[22] T. Yao, Y. Oka, and N. Yamamoto, J. Mater. Chem. **2**, 331 (1992).
[23] T. Yao, Y. Oka, and N. Yamamoto, J. Mater. Chem. **2**, 337 (1992).
[24] S. Andersson, Acta Chem. Scand. (1947-1973) **19**, 1371 (1965).
[25] D. B. Le, S. Passerini, J. Guo, J. Ressler, B. B. Owens, and W. H. Smyrl, J. Electrochem. Soc. **143**, 2099 (1996).
[26] W. Dong, D. R. Rolison, and B. Dunn, Electrochem. Solid-State Lett. **3**, 457 (2000).

[27] J. Livage, Chem. Mater. **3**, 578 (1991).

[28] WINEPR SIMFONIA Ver. 1.25, Bruker Analytische Messtechnik GmbH (1996).

[29] D. Fenzke, D. Freude, T. Fröhlich, and J. Haase, Chem. Phys. Lett. **111**, 171 (1984).

[30] P. C. Taylor, J. F. Baugher, and H. M. Kriz, Chem. Rev. **75**, 203 (1975).

[31] V. H. Schmidt, in *Proceedings of Ampere International Summer School II*, edited by R. Blinc (University of Ljubljana Press, Ljubljana, Yugoslavia, 1972).

[32] R. J. Cava, A. Santoro, D. W. Murphy, S. M. Zahurak, R. M. Fleming, P. Marsh, and R. S. Roth, J. Solid State Chem. **65**, 63 (1986).

[33] P. E. Stallworth, S. Kostov, M. L. denBoer, S. G. Greenbaum, C. Lampe-Onnerud, J. Appl. Phys. **83**, 1247 (1998).

[34] N. Bloembergen, E. M. Purcell, and R. V. Pound, Phys. Rev. **73**, 679 (1948).

[35] S. D. Gornostansky and C. V. Stager, J. Chem. Phys. **46**, 4959 (1967).

[36] S. Hayakawa, T. Yoko, and S. Sakka, J. Solid State Chem. **112**, 329 (1994).

[37] A. A. Shubin, O. B. Lapina, E. Bosch, J. Spengler, and H. Knözinger, J. Phys. Chem. B **103**, 3138 (1999).

[38] G. F. Lynch, S. L. Segel, and M. Sayer, J. Magn. Reson. (1969-1992) **15**, 8 (1974).

[39] A. F. Wells, *Structural Inorganic Chemistry*, 3rd ed. (Oxford University Press, London, 1962).

[40] P. A. Cox, *The Electronic Structure and Chemistry of Solids* (Oxford University Press, London, 1987).

[41] P. Hertel and J. Appel, Phys. Rev. B **33**, 2098 (1986).

[42] M. Rubinstein, Phys. Rev. B **2**, 4731 (1970).

[43] J. Winter, *Magnetic Resonance in Metals* (Oxford University Press, London, 1971).

[44] H. G. Hecht and T. S. Johnston, J. Chem. Phys. **46**, 23 (1967).

[45] O. B. Lapina, A. A. Shubin, A. V. Nosov, E. Bosch, J. Spengler, and H. Knözinger, J. Phys. Chem. B **103**, 7599 (1999).

[46] P. J. Carl, S. L. Isley, and S. C. Larsen, J. Phys. Chem. A **105**, 4563 (2001).

[47] M. Giorgetti, S. Passerini, W. H. Smyrl, and M. Berrettoni, Chem. Mater. **11**, 2257 (1999).

[48] E. R. Andrew and D. P. Tunstall, Proc. Phys. Soc. London **78**, 1 (1961).